Transforming the Self-Assembled Structures of Diblock Copolymer/POSS Nanoparticle Composites Through Complementary Multiple Hydrogen Bonding Interactions

Yu-Rong Wu, Yi-Chen Wu, Shiao-Wei Kuo*

Well-defined self-assembled structures are obtained in the form of block copolymer (BCP) nanocomposites, prepared by blending octuply adenine (A)-functionalized polyhedral oligomeric silsesquioxane (OBA-POSS) nanoparticles (NPs) with a thymine (T)-containing BCP (PS-*b*-PVBT); these nanocomposites are stabilized through complementary multiple hydrogen bonding interactions between the A and T units. A transition from one ordered morphology to another occurs upon increasing the content of OBA-POSS NPs in the PS-*b*-PVBT diblock copolymer, namely lamellar structures at relatively low OBA-POSS NP contents (<25 wt%) and cylindrical structures at higher OBA-POSS NP contents (>25 wt%), with concomitant variations in the effective interaction parameter and the overall volume fractions of the two microphase-separated domains.

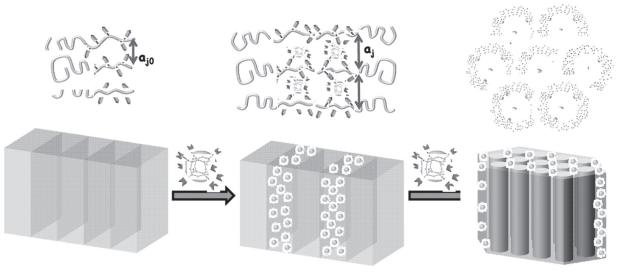

1. Introduction

The preparation of block copolymer/nanoparticle (BCP/NP) composites is motivated by the intriguing opportunity to engineer novel properties from combinations of the individual components' particular electronic, optical, and magnetic properties.[1–4] Diblock copolymers can form a variety of self-assembled nanostructures, including spheres, cylinders, lamellae, and bicontinuous gyroids, with characteristic length scales in the range from 10 to 100 nm.[5,6] The type of structure is strongly dependent on the volume fraction of one block relative to the other. The blending of diblock copolymers with NPs can create composites exhibiting novel optical and mechanical properties derived from the NPs themselves, with the distribution of NPs in the microphase-separated morphologies of BCPs leading to hierarchically structured composites.[7–10] Polymer nanocomposites with hierarchical structures may provide unexpected improvements in material stiffness, strength, and heat resistance; BCP/NP blends are also fascinating model systems for studying the mechanisms of structure formation from soft/hard heterogeneous materials.[11]

In general, the use of ligands that are compatible with only one of the block can lead to preferential segregation of the NPs within the compatible domain. For example, Kramer and co-workers[12-16] controlled the distribution of NPs in microphase-separated structures of polystyrene-*block*-poly(2-vinyl pyridine) (PS-*b*-P2VP) BCPs by using PS or P2VP homopolymers as ligands. In such a system in which the ligand is chemical identical to one of the blocks, the addition of each enthalpically neutral particle carries an entropic penalty that pushes the system close to disorder at higher volume fractions of the NPs. Recently, hydrogen bonding has been adopted to blend BCPs and homopolymers, significantly enhancing the miscibility and swelling of the BCP domain without macrophase separation or corresponding transitions

Y.-R. Wu, Y.-C. Wu, Prof. S.-W. Kuo
Department of Materials and Optoelectronic Science, Center for Nanoscience and Nanotechnology, National Sun Yat-Sen University, Kaohsiung, Taiwan
E-mail: kuosw@faculty.nsysu.edu.tw

DOI: 10.1002/macp.201300251

from one ordered morphology to another.[17–26] This behavior is similar to that found in BCP/NP systems.[27–37] For example, Wei and co-workers[27,28] obtained simple cubic structures from composites of polystyrene-*block*-poly(ethylene oxide) and CdS NPs when combining an originally hexagonally packed cylindrical PS-*b*-PEO structure with CdS NPs modified on their surfaces with EtOH functional groups. These modified CdS NPs tethered selectively to the PEO chains through hydrogen bonds, becoming well dispersed within the PEO domains of the PS-*b*-PEO copolymer.[27,28] Similar results have been found for blends of PS-*b*-P4VP and modified CdS NPs, stabilized through hydrogen bonding between the pyridyl groups of P4VP and the OH groups on the surface of the NPs.[29] When blending PS-*b*-P4VP with OH-capped CdSe NPs, Matsushita and co-workers[35] observed domain spacing expansion and a morphological transition upon addition of the CdSe NPs as a result of hydrogen bonding between the pyridyl groups of P4VP and the OH groups on the surface of the NPs. Watkins and co-workers[34] reported that higher loadings of NPs based on functionalized polyhedral oligomeric silsesquioxanes (POSS) were possible within polyethylene oxide-*block*-polypropylene oxide-*block*-poly(ethylene oxide) triblock copolymers; POSS NPs presenting maleamic acid or aminophenyl groups as ligands enabled selective hydrogen bonding with the PEO domains; further addition of the additive induced an ordered–ordered transition between cylindrical and spherical morphologies. The NP-induced transformations of other self-assembled A-*block*-B structures have been investigated in several previous studies,[27–37] essentially all of which involved systems where the NPs were immiscible with block A but interacted favorably with block B. In general, these interactions have been formed through single-site hydrogen bonding of an OH group of an NP with a pyridyl group of P4VP or an ether group of PEO; these interactions are relatively weaker than the multiple hydrogen bonding interactions formed in DNA-like complexes (e.g., adenine (A) interacting with thymine (T) or guanine (G) with cytosine (C)).[38–40] We suspect that stronger multiple hydrogen bonding interactions might enable higher loadings of NPs in a diblock copolymer matrix.

In this study, we report a new system in which polystyrene-*block*-poly(4-vinylbenzyl triazolylmethyl methylthymine) (PS-*b*-PVBT) transforms from a lamellar structure to a hexagonally packed cylinder structure at particularly high loadings (>60 wt%) of octakis(vinylbenzyladenine-siloxy)silsesquioxane (OBA-POSS) NPs. In this system, the OBA-POSS NPs are miscible with the PVBT blocks, stabilized through multiple hydrogen bonding interactions between the A and T units, but are immiscible with the PS blocks. POSS compounds, unique cage-like structures possessing nanoscale dimensions, are particularly interesting components for the preparation of hybrid materials. These inorganic/organic hybrid architectures contain an inner inorganic framework composed of silicon and oxygen atoms $[(SiO_{1.5})_x]$ surrounded by organic substituents.[41–47] OBA-POSS possesses eight A groups, which form multiple hydrogen bonds with the T groups of PVBT blocks. The interassociation equilibrium constant for the interaction between A and T (ca. 530 M^{-1}) is significantly higher than those (ca. 10 M^{-1}) usually found for OH···O=C or OH···ether single-site hydrogen bonding.[48] In this study, we used differential scanning calorimetry (DSC), wide-angle X-ray diffraction (WAXD), transmission electron microscopy (TEM), small-angle X-ray scattering (SAXS), and Fourier transform infrared (FTIR) spectroscopy to characterize the self-assembly of and specific interactions in PS-*b*-PVBT/OBA-POSS hybrids.

2. Experimental Section

2.1. Materials

The PS_{87}-*b*-$PVBT_{22}$ ($\overline{M}_n$ = 16 400 g mol^{-1}; PDI = 1.20) copolymer, a T-containing BCP, was synthesized through nitroxide-mediated radical polymerization of polystyrene-*block*-poly(4-vinylbenzyl azide) (PS-*b*-$PVBN_3$) and subsequent click reactions with propargylthymine.[49] Octakis(vinylbenzyladenine-siloxy)silsesquioxane (OBA-POSS; $\overline{M}_n$ = 2947 g mol^{-1}) was prepared through the reaction of A with octakis(benzyl chloride)–POSS (OVBC–POSS), itself prepared through hydrosilylation of octakis(dimethylsiloxy) silsesquioxane ($Q_8M_8^H$) with vinyl benzyl chloride.[50] Details of the synthesis and characterization of PS-*b*-PVBT and OBA-POSS are available elsewhere.[50,51] ^{1}H NMR of PS-*b*-PVBT (d_6-DMSO, δ_H): 4.87 (2H, NCHC**H**$_2$ N), 5.45 (2H, Ar**CH**$_2$ N), 6.29, 6.90 (9H, **ArH**), 7.54 (2H, ArCH$_2$N**CH**CCH$_2$N), 8.14 [1H, N**CH**C(CH$_3$)CO], 11.31 (1H, T **NH**). ^{13}C NMR of PS-*b*-PVBT (d_6-DMSO) δ_C: 11.82 [NCHC(**C**H$_3$)CO], 31.04, 42.43 (**C**H$_2$ **C**H$_2$Ar), 36.10 (ArCH$_2$NCHC**C**H$_2$N), 52.63 (Ar**C**H$_2$N), 109.14 [NCH**C**(CH$_3$)CO], 123.57 (ArCH$_2$N**C**HCCH$_2$), 127.53, 132.40, 150.89 (Ar), 141.20 [N**C**HC(CH$_3$)CO], 142.98 (ArCH$_2$NCH**C**CH$_2$), 162.44 (NH**C**ON), 164.73 (NH**C**OC). MALDI–TOF mass of OBA-POSS (calcd. 2947). ^{1}H NMR of OBA-POSS (DMSO, ppm): δ 5.31 (s, 2H), 8.16 (s, 2H, NH$_2$), 8.22 (s, 1H), 3.54 (s, 2H). ^{13}C NMR (DMSO, δ): 45.9, 118.7, 144.1, 149.5, 152.6, 156.0. FTIR of OBA-POSS (KBr): 3317, 3157 (NH str.), 2959, 2844 (aliphatic CH str.), 1062 (SiOSi), 1652 (C=N str.), 1601 cm^{-1} (NH def.). Elemental analysis: anal. calcd. for OBA-POSS C 44.18, H 3.94, N 18.41; found: C 56.82, H 6.49, N 19.40.

2.2. BCP/NP Blends

Blend samples containing various weight fractions of PS-*b*-PVBT and OBA-POSS were prepared through solution casting. A dimethylformamide (DMF) solution containing 5 wt% of the blend was stirred for 8–10 h and then cast on a polytetrafluoroethylene (Teflon) dish. The solvent was evaporated slowly at 80 °C for 1 d and then the sample was dried in a vacuum oven at 120 °C for 4 d.

2.3. Characterization

The thermal properties of the BCP/NP blend films were determined through DSC analysis using a TA Q-20 instrument; the scan rate was 20 °C min^{-1} within the temperature range 0–250 °C. The glass transition temperature (T_g) is defined herein as the midpoint of the heat capacity transition between the upper and lower points of deviation from the extrapolated liquid and glass lines. FTIR spectra of the polymer blend films were recorded using the conventional KBr disk method with a Bruker Tensor 27 FTIR spectrophotometer (32 scans; spectral resolution: 1 cm^{-1}); the films were sufficiently thin to obey the Beer–Lambert law. SAXS data were collected using the BL17A1 wiggler beamline of the National Synchrotron Radiation Research Center (NSRRC), Taiwan. All temperature-resolved SAXS measurements were carried out at several temperatures on a hot-stage under a dry-nitrogen atmosphere. The samples were sealed between two Kapton windows (thickness: 12 μm). An X-ray beam having a diameter of 0.5 mm and a wavelength (λ) of 1.1273 $Å^{-1}$ was used for the SAXS measurements (Q range: 0.015–0.3 $Å^{-1}$). TEM experiments were conducted using a JEOL 2100 microscope (Japan) operated at 200 kV. Ultrathin sections of the samples were prepared using a Leica Ultracut S microtome equipped with a diamond knife. Slices (thickness: ca. 700 Å) were cut at room temperature. The ultrathin sections of the PS-*b*-PVBT/OBA-POSS hybrids were placed onto copper grids coated with carbon supporting films.

3. Results and Discussion

Figure 1 displays conventional second-run DSC thermogram images, obtained at a heating rate of 20 °C min^{-1}, of PS-*b*-PVBT/OBA-POSS hybrids of various compositions. The T_g of pure OBA-POSS, which also features strong, self-complementary, multiple hydrogen bonding interactions, is higher than that of a similar octakis-functionalized POSS-lacking multiple hydrogen bonding interactions.[38] In addition, the endothermic peak near 150 °C for pure OBA-POSS corresponds to the melting of the POSS moieties.[52–54] The pure PS-*b*-PVBT BCP displayed two T_gs because two different types of segments are present in the polymer chain. Our DSC analysis revealed that the lower value of T_g of the PS-*b*-PVBT BCP occurred near 108 °C, indicating a large presence of PS segments. We assign the higher value of T_g (ca. 165 °C) to the PVBT segments in the copolymer. Notably, the value of T_g of the PS block (108 °C) of the PS-*b*-PVPBT copolymer is higher than that of the PS homopolymer (ca. 100 °C at the same molecular weight), due to the hard confinement of the PVBT block (T_g = 165 °C). The value of T_g of the PVBT block decreased significantly, whereas that of the PS block remained almost unchanged (decreased only slightly), upon increasing the content of OBA-POSS. Therefore, we suspected that the added OBA-POSS NPs interacted preferentially with the PVBT blocks through multiple hydrogen bonding interactions of their A and T units. At lower contents of the OBA-POSS NPs

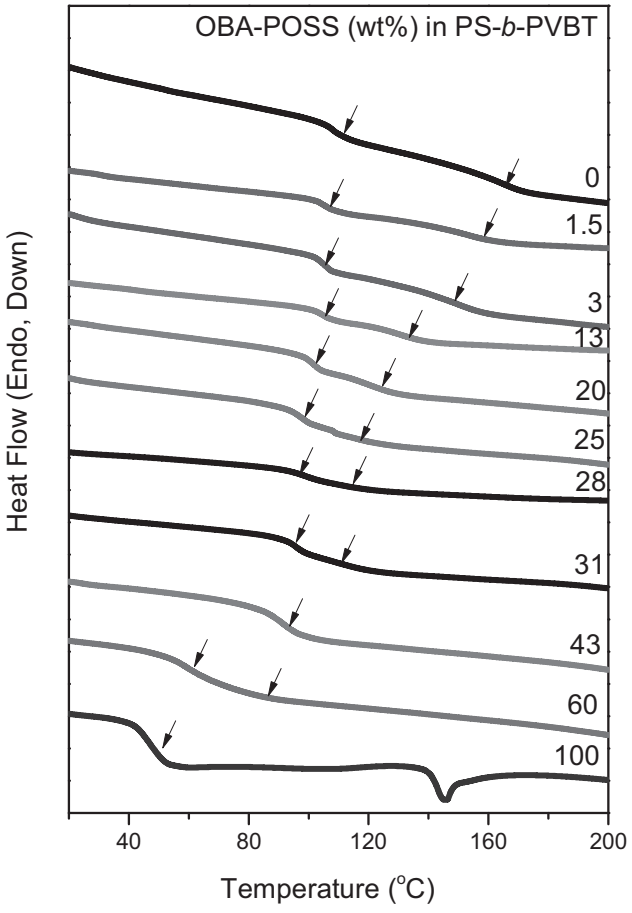

Figure 1. DSC thermogram images of PS-*b*-PVBT/OBA-POSS NP hybrids.

(<31 wt%), we observed two values of T_g; we assign the lower (ca. 96–108 °C) to a PS-dominant phase, which had phase-separated from the PVBT/OBA-POSS hybrid complex, and the higher (ca. 111–160 °C) to the phase of a multiple hydrogen bonded PVBT/OBA-POSS hybrid complex. The depression of the glass transition behavior in the PS domains was probably due to the lowering of the value of T_g of the PVBT/OBA-POSS domains (i.e., more flexible chains) upon increasing the content of OBA-POSS NPs. At a relatively high content of OBA-POSS NPs (43 wt%), we detected only a single, but broad, endothermic event near 94 °C. Here, we suspect that the glass transition of the miscible PVBT/OBA-POSS microphase had, by coincidence, dropped to the same temperature range as that of the PS segment, such that the two could not be resolved. A further increase in the content of OBA-POSS NPs to 60 wt% caused the two glass transitions to reappear: the lower (ca. 64 °C) was due to the multiple hydrogen bonded PVBT/OBA-POSS hybrid complex and the higher (ca. 90 °C) was due to the PS domains, as would be expected. Figure 2 summarizes the glass transition behavior of the PS-*b*-PVBT/OBA-POSS hybrid complexes. Interestingly, the values of T_g of the

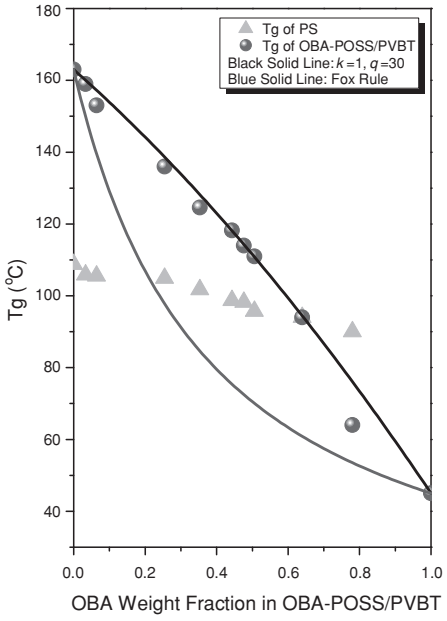

Figure 2. Glass-transition behavior of the PS and PVBT/OBA-POSS phases at various OBA-POSS contents.

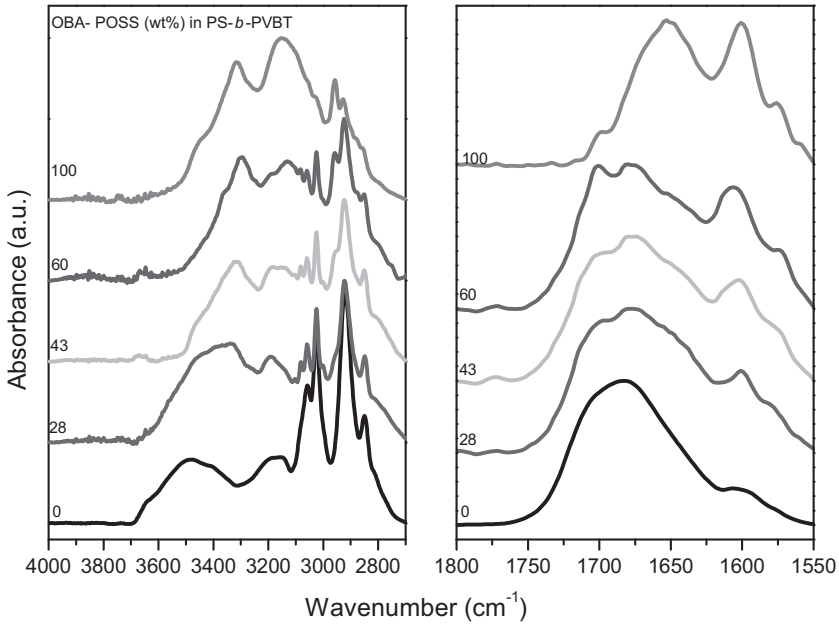

Figure 3. FTIR spectra, recorded at room temperature, of PS-*b*-PVBT/OBA-POSS NP hybrids of various compositions: a) NH and b) C=O stretching regions.

PVBT/OBA-POSS hybrid complex domain exhibited a positive deviation from the Fox and linear rules. In addition, the Kwei equation[55] is usually employed to characterize systems displaying specific interactions:

$$T_g = \frac{W_1 T_{g1} + kW_2 T_{g2}}{W_1 + kW_2} + qW_1 W_2 \quad (1)$$

where W_1 and W_2 are the weight fractions of the components, T_{g1} and T_{g2} are the corresponding glass transition temperatures, and k and q are fitting constants. The parameter q represents the strength of the specific interactions in the system; it reflects a balance between the breaking of self-association interactions and the forming of inter-association interactions. From nonlinear least-squares "best fits" of the plots for the PA-T/OBA-POSS complexes, we obtained values of k and q of 1 and 30, respectively. A positive value of q usually suggests that intercomplementary multiple hydrogen bonding in PVBT/OBA-POSS hybrid complex was stronger than the self-complementary multiple hydrogen bonds (T···T and A···A) in PVBT and OBA-POSS, respectively.

Infrared spectroscopy is a highly effective method for investigating multiple hydrogen bonding interactions in supramolecular polymer complexes.[56] At room temperature, the complementary multiple hydrogen bonding between PS-*b*-PVBT and OBA-POSS is strong. The FTIR spectra in Figure 3 confirm the existence of multiple hydrogen bonds between the PS-*b*-PVBT copolymer and the OBA-POSS NPs. The stretching vibrations of the free and hydrogen-bonded NH groups of the pure PS-*b*-PVBT appear as characteristic peaks at 3500 and 3172 cm^{-1}, respectively. The intensity of the free amide NH stretching vibration at 3500 cm^{-1} decreased upon increasing the amount of added OBA-POSS, indicating that PS-*b*-PVBT associated strongly with its complement OBA-POSS; the signal in the NH stretching region of the PS-*b*-PVBT and OBA-POSS mixture, where the band at 3500 cm^{-1} corresponds to free NH stretching, shifted to 3300 cm^{-1}, attributable to the A groups interacting with the T units.[57,58] In addition, a peak appeared at 3200 cm^{-1} that corresponded to the NH groups in the T units interacting with the A moieties.[58] Upon increasing the content of OBA-POSS, we also observed growing signals (near 1676 cm^{-1}) for the multiple hydrogen bonding interactions of the C=O groups of the T units with the NH_2 groups of the A units and for the pyridyl groups of the A moieties interacting with the NH groups of the T moieties.

Figure 4a–d display SAXS profiles of PS-*b*-PVBT/OBA-POSS hybrid complexes of various compositions at different temperatures. The PS-*b*-PVBT/OBA-POSS hybrid complexes at 30 °C exhibited a broad primary scattering peak (q_{max}) for all compositions; hints of ordered scattering peaks for 1.5 and 3 wt% of OBA-POSS at q/q_{max} ratios of 2 and 4, respectively (Figure 4a and b, respectively); and also hints of ordered scattering peaks for the 28 and 43 wt% OBA-POSS samples at a ratio q/q_{max} of √3 in Figure 4c and d, respectively. At 180 °C, the samples were fully annealed and well ordered, as indicated by the sharp primary scattering peak and well-defined higher

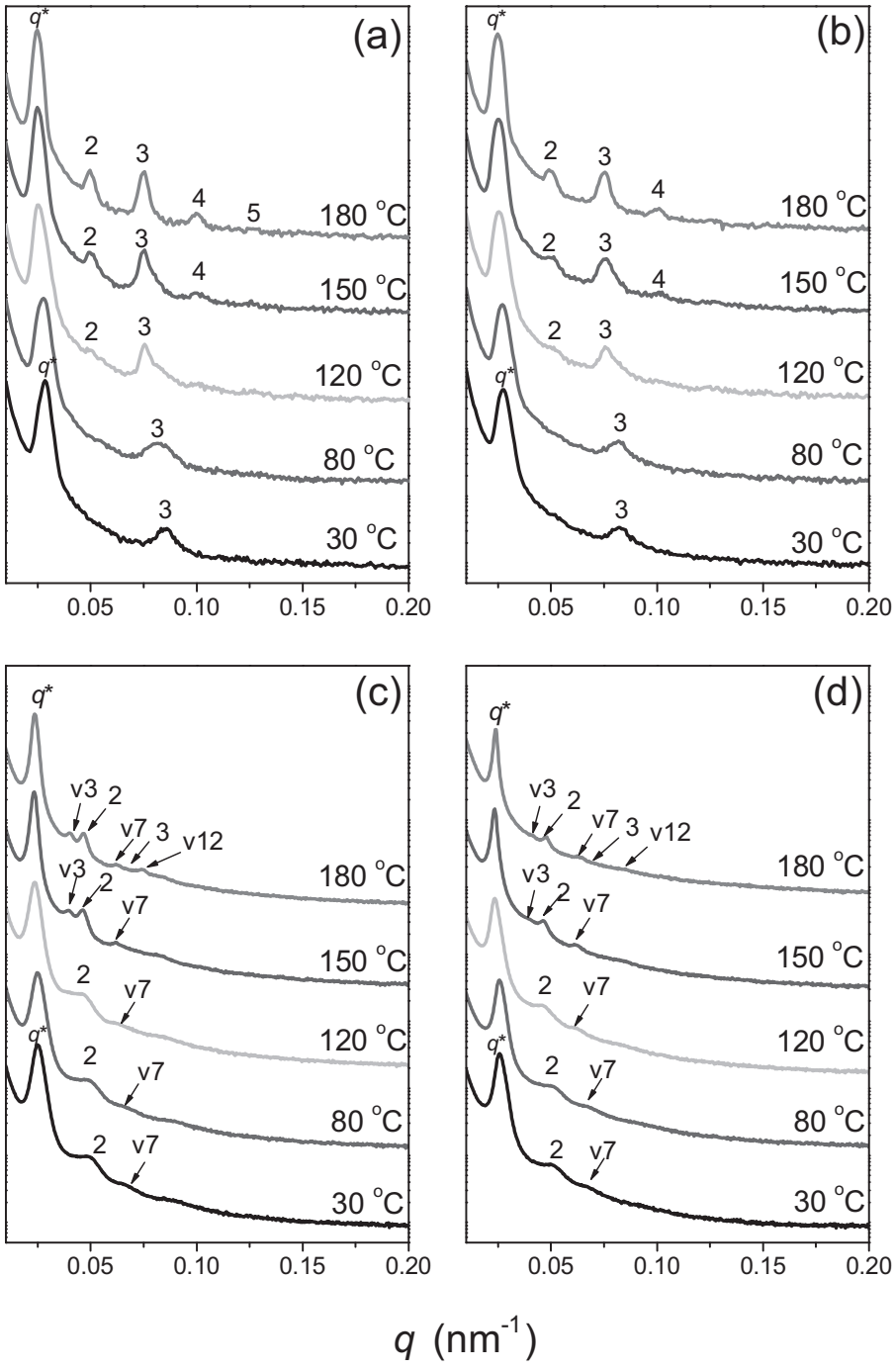

Figure 4. a–d) SAXS patterns of PS-*b*-PVBT/OBA-POSS hybrid complexes at various temperatures [OBA-POSS NP contents: a) 1.5, b) 3, c) 28, and d) 43 wt%]

peaks for the 1.5 and 3 wt% OBA-POSS blends at q/q_{max} ratios of 2, 3, 4, and 5 (Figure 4a and b, respectively), corresponding to the long-range order of lamellar structures. In addition, the well-defined higher peaks for the 28 and 43 wt% OBA-POSS samples appeared at q/q_{max} ratios of √3, √4, √7, √9, and √12 (Figures 4c and d, respectively), corresponding to the long-range order of cylindrical structures. Figure 5 summarizes the data for the PS-*b*-PVBT/OBA-POSS hybrid complexes of various compositions at 180 °C. SAXS analysis revealed a lamellar microdomain structure for the pure PS-*b*-PVBT diblock copolymer – judging from the scattering maxima at relative positions of 1:2:3:4:5, corresponding to a domain spacing of 24.6 nm ($q = 0.0255$ nm^{-1}) – that was associated

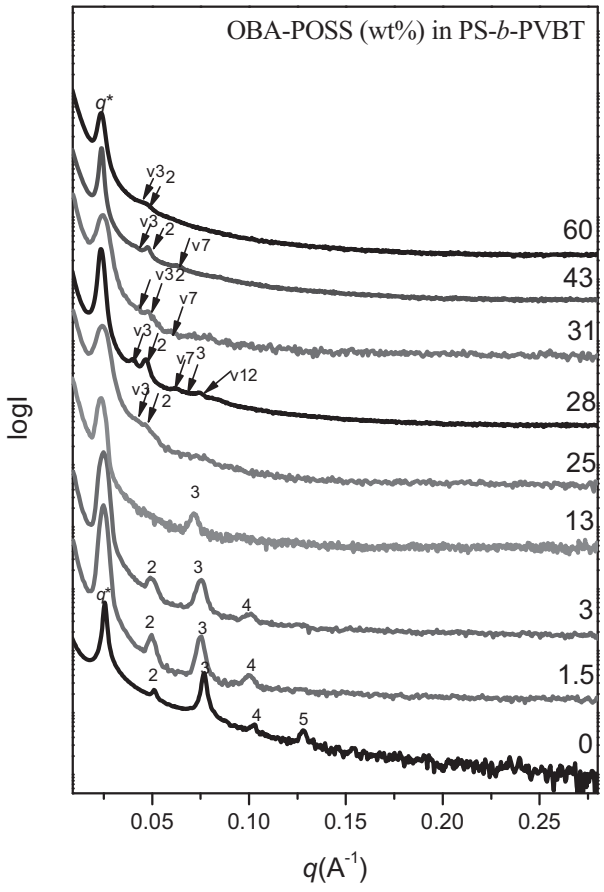

Figure 5. SAXS patterns of PS-*b*-PVBT/OBA-POSS hybrid complexes of various compositions at 180 °C.

with the larger-scale copolymer domain structure arising from microphase separation of the PS and PVBT blocks. The TEM image in Figure 6a for pure PS-*b*-PVBT (staining with RuO_4) is consistent with the SAXS analysis data, which reveal the long-range order of a lamellar structure. Weak-intensity peaks at relative values of q of 2 and 4 suggest that the composition of one phase in the lamellae was close to 0.5[59] when the volume fraction of the PS phases in the lamellar structure was 64% for this diblock copolymer.[50] The addition of 1.5 and 3 wt% of OBA-POSS NPs resulted in obvious second and fourth peaks, also suggesting a lamellar morphology, as confirmed in the TEM images in Figure 6b and c. In addition, the first-order scattering position shifted slightly to the lower-q region upon increasing the OBA-POSS content (e.g., at 13 wt%: $q_{max} = 0.0239$ nm^{-1}; d-spacing = 26.2 nm), indicating an increase in the interlamellar spacing D. We also observe that the even-order peaks disappeared at an OBA-POSS NP content of 13 wt%, resulting from the structure factors of the lamellae, implying that the volume fractions of the PS and PVBT/OBA-POSS phases were almost equal ($f^{v}_{PS} = 0.55$ in this case). Interestingly, upon increasing the content of OBA-POSS NPs to 25 wt%, a transition occurred from lamellar to cylindrical structures with a d-spacing of 25.9 nm. This additive-induced ordered–ordered morphological transition was driven by both increases in the effective interaction parameter and changes in the overall volume fraction between the two microphase-separated domains. Further increasing the content of OBA-POSS NPs did not change the peak ratios

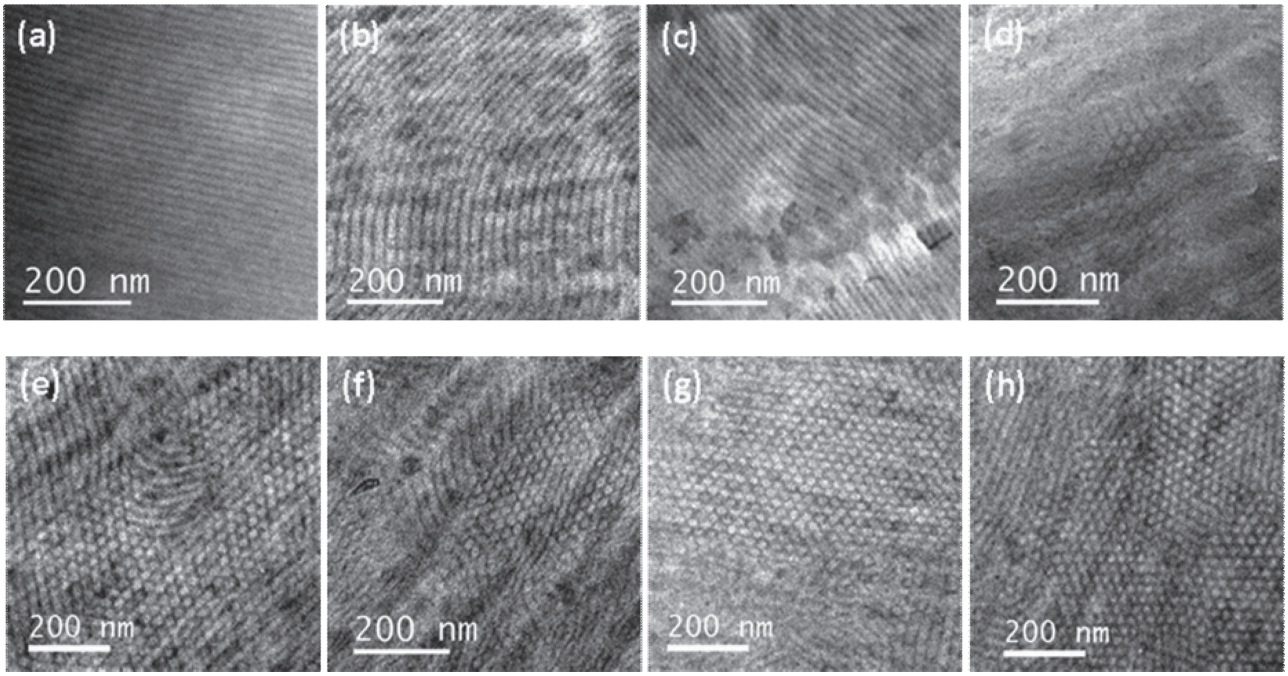

Figure 6. TEM images of PS-*b*-PVBT/OBA-POSS hybrid complexes at OBA-POSS NP contents of a) 0, b) 1.5, c) 3, d) 25, e) 28, f) 31, g) 43, and h) 60 wt%.

in the SAXS patterns, which revealed the 1:√3:√4:√7:√9:√12 ratio expected for long-range order of cylindrical structures; this behavior is confirmed in the TEM images in Figure 6d–h and the only slight increase in the *d*-spacing to 26.4 nm for an OBA-POSS NP content of 60 wt%. Here, the TEM images in Figure 6b–h obtained without any staining, we attribute the dark regions to POSS-rich layers because the Si atoms of POSS provide a high mass contrast relative to the organic domains. In the minor domain, the bright regions correspond to the PS phase and the dark regions correspond to the mixed phase of PVBT/OBA-POSS NPs. We were also interested in examining how the OBA-POSS NPs were distributed in this hybrid. The correlated changes in the average distance a_J of the chemical junctions along the interface – and, therefore, the relative changes a_J/a_{J0} (where a_{J0} represents the value for the pure BCP) – can be derived for the complexes. Simple volumetric conservation leads to values of D/D_0 of $(\rho_J/\rho_{J0})\Phi_{block}^{-1}$ for a lamellar structure and $(\rho_J/\rho_{J0})[(2/3^{1/2})\pi\Phi_{block}^{-1}]^{1/2}$ for a hexagonally packed cylindrical structure, where D_0 is the interdomain distance of pure PS-*b*-PVBT (D_0 = 24.6 nm) and ρ_J is the number of block chains per unit interfacial area (ca. a_J^{-2}); therefore, a_J/a_{J0} is approximately equal to $(\rho_J/\rho_{J0})^{-1/2}$ and Φ is the volume fraction of the BCP in the hybrid, as suggested by Hashimoto and co-workers.[60,61] Based on these relations, we found that the values of a_J/a_{J0} for our hybrid complexes increased from 1.03 to 1.43 to 1.67 upon increasing the OBA-POSS NPs content (from 13 to 25 to 60 wt%, respectively). We surmise that the added OBA-POSS NPs interacted with the PVBT chains of the BCP through complementary multiple hydrogen bonds at the interfaces, resulting in the observed expansion in the values of a_J. The PS blocks, being chemically linked to the PVBT blocks, had to contract to accommodate the expanded interfacial zone and we recommend the assumption of no density change in BCP/NPs hybrids. In addition, we suspect that the bound PVBT/OBA-POSS hybrid complex simply had a reduced enthalpic cost at the interface. This behavior is commonly observed upon the addition of NPs – they increase the interface per chain by "hiding" the blocks from each other. Scheme 1 plots the morphological transformation of the PS-*b*-PVBT BCP that occurred upon increasing the OBA-POSS NP content. Pure PS-*b*-PVBT BCP exhibited the long-range order of a lamellar structure. OBA-POSS NPs contents of up to 25 wt% retained the lamellar structure; further increasing the content of OBA-POSS NPs to greater than 25 wt% resulted in the ordered–ordered morphological transition from lamellar to cylindrical structures, due to the complementary multiple hydrogen bonding interactions formed between A and T units in the PVBT/OBA-POSS hybrid complex and changes in the overall volume fractions of the two microphase-separated domains.

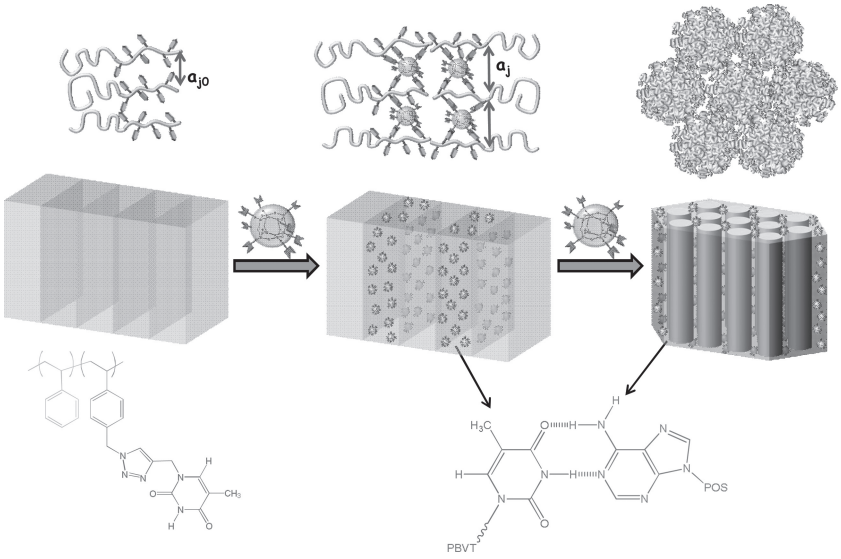

Scheme 1. Morphological changes in hybrid complexes of PS-*b*-PVBT upon increasing the content of OBA-POSS NPs.

4. Conclusion

We have used DSC, TEM, SAXS, and FTIR spectroscopy to investigate, in detail, the miscibility, phase behavior, and hydrogen bonding interactions of hybrid complexes formed between PS-*b*-PVBT and OBA-POSS NPs. The self-assembled structures of the BCP composites depended significantly on the content of OBA-POSS, transforming from lamellar structures at relative low contents of OBA-POSS NPs to cylindrical structures at relatively high contents of OBA-POSS NPs, even at 60 wt%. These results suggest that complementary multiple hydrogen bonding interactions might be a useful tool for designing BCP/NP hybrids exhibiting interesting optical, electrical, and magnetic properties.

Acknowledgements: This study was supported financially by the National Science Council, Taiwan, Republic of China, under contracts NSC 100-2221-E-110-029-MY3 and NSC 100-2628-E-110-001.

Received: March 15, 2013; Revised: April 17, 2013; Published online: June 10, 2013; DOI: 10.1002/macp.201300251

Keywords: self-assembly; hydrogen bonding; composite materials; diblock copolymers; nanoparticles

[1] A. C. Balazs, T. Emrick, T. P. Russell, *Science* **2006**, *314*, 1107.
[2] J. Y. Cheng, C. A. Ross, V. Z. H. Chan, E. L. Thomas, R. G. H. Lammertink, G. J. Vancso, *Adv. Mater.* **2001**, *13*, 1174.
[3] T. F. Jaramillo, S. H. Baeck, B. R. Cuenya, E. W. McFarland, *J. Am. Chem. Soc.* **2003**, *125*, 7148.
[4] S. C. Warren, L. C. Messina, L. S. Slaughter, M. Kamperman, Q. Zhou, S. M. Gruner, F. J. Disalve, U. Wiesner, *Science* **2008**, *320*, 1748.
[5] L. Zhu, S. Z. D. Cheng, P. Huang, Q. Ge, R. P. Quirk, E. L. Thomas, B. Lotz, B. S. Hsiao, F. Yeh, L. Liu, *Adv. Mater.* **2002**, *14*, 31.
[6] J. Z. Zhang, *Acc. Chem. Res.* **1997**, *30*, 423.
[7] M. R. Hammond, H. Dietsch, O. Pravaz, P. Schurtenberger, *Macromolecules* **2011**, *43*, 8340.
[8] S. Barrau, T. Heiser, F. Richard, C. Brochon, C. Ngov, K. Vande Wetering, G. Hadziioannou, D. V. Anokhin, D. A. Ivanov, *Macromolecules* **2008**, *41*, 2701.
[9] C. Yang, J. K. Lee, A. J. Heeger, F. Wudl, *J. Mater. Chem.* **2009**, *19*, 5416.
[10] A. Urbas, R. Sharp, Y. Fink, E. L. Thomas, M. Xenidou, L. J. Fetters, *Adv. Mater.* **2000**, *12*, 812.
[11] M. R. Bockstaller, Y. Lapetnikov, S. Margel, E. L. Thomas, *J. Am. Chem. Soc.* **2003**, *125*, 5276.
[12] J. J. Chiu, B. J. Kim, E. J. Kramer, D. J. Pine, *J. Am. Chem. Soc.* **2005**, *127*, 5036.
[13] B. J. Kim, J. Bang, C. J. Hawker, E. J. Kramer, *Macromolecules* **2006**, *39*, 4108.
[14] S. C. Park, B. J. Kim, C. J. Hawker, E. J. Kramer, J. Bang, J. S. Ha, *Macromolecules* **2007**, *40*, 8119.
[15] J. J. Chiu, B. J. Kim, G. R. Yi, J. Bang, E. J. Kramer, D. J. Pine, *Macromolecules* **2007**, *40*, 3361.
[16] B. J. Kim, G. H. Fredrickson, E. J. Kramer, *Macromolecules* **2008**, *41*, 436.
[17] H. F. Lee, S. W. Kuo, C. F. Huang, J. S. Lu, S. C. Chan, C. F. Wang, F. C. Chang, *Macromolecules* **2006**, *39*, 5458.
[18] Y. Matsushita, *Macromolecules* **2007**, *40*, 771.
[19] N. Hameed, Q. Guo, *Macromolecules* **2008**, *41*, 7596.
[20] K. Dobrosielska, S. Wakao, A. Takano, Y. Matsushita, *Macromolecules* **2008**, *41*, 7695.
[21] K. Dobrosielska, S. Wakao, J. Suzuki, K. Noda, A. Takano, Y. Matsushita, *Macromolecules* **2009**, *42*, 7098.
[22] W. C. Chen, S. W. Kuo, U. S. Jeng, F. C. Chang, *Macromolecules* **2008**, *41*, 1401.
[23] W. C. Chen, S. W. Kuo, C. H. Lu, F. C. Chang, *Macromolecules* **2009**, *42*, 3580.
[24] I. H. Lin, S. W. Kuo, F. C. Chang, *Polymer* **2009**, *50*, 5276.
[25] S. C. Chen, S. W. Kuo, U. S. Jeng, C. J. Su, F. C. Chang, *Macromolecules* **2010**, *43*, 1083.
[26] S. W. Kuo, *Polym. Int.* **2009**, *58*, 455.
[27] U. S. Jeng, Y. S. Sun, H. J. Lee, C. H. Hsu, K. S. Liang, S. W. Yeh, K. H. Wei, *Macromolecules* **2004**, *37*, 4617.
[28] S. W. Yeh, K. H. Wei, Y. S. Sun, U. S. Jeng, K. S. Liang, *Macromolecules* **2003**, *36*, 7903.
[29] S. W. Yeh, K. H. Wei, Y. S. Sun, U. S. Jeng, K. S. Liang, *Macromolecules* **2005**, *38*, 6559.
[30] C. H. Lu, S. W. Kuo, W. T. Chang, F. C. Chang, *Macromol. Rapid Commun.* **2009**, *30*, 2121.
[31] S.W. Kuo, H. Y. Yang, *Macromol. Chem. Phys.* **2011**, *212*, 2249.
[32] S. G. Jang, E. J. Kramer, C. J. Hawker, *J. Am. Chem. Soc.* **2011**, *133*, 16986.
[33] Y. Lin, V. K. Daga, E. R. Anderson, S. P. Gido, J. J. Watkins, *J. Am. Chem. Soc.* **2011**, *133*, 6513.
[34] V. K. Daga, E. R. Anderson, S. P. Gido, J. J. Watkins, *Macromolecules* **2011**, *44*, 6793.
[35] A. Noro, K. Higuchi, Y. Sageshima, Y. Matsushita, *Macromolecules* **2012**, *45*, 8013.
[36] S. G. Jang, A. Khan, C. J. Hawker, E. J. Kramer, *Macromolecules* **2012**, *45*, 1553.
[37] T. Lin, R. M. Ho, J. C. Ho, *Macromolecules* **2009**, *42*, 742.
[38] J. R. Smith, *Prog. Polym. Sci.* **1996**, *21*, 209.
[39] S. W. Kuo, S. T. Tsai, *Macromolecules* **2009**, *42*, 4701.
[40] Y. C. Wu, S. W. Kuo, *J. Mater. Chem.* **2012**, *22*, 2982.
[41] S. W. Kuo, F. C. Chang, *Prog. Polym. Sci.* **2011**, *36*, 1649.
[42] H. Xu, S. W. Kuo, J. S. Lee, F. C. Chang, *Macromolecules* **2002**, *35*, 8788.
[43] H. C. Lin, S. W. Kuo, C. F. Huang, F. C. Chang, *Macromol. Rapid Commun.* **2006**, *27*, 537.
[44] B. B. Jiang, W. Tao, X. Lu, Y. Liu, H. B. Jin, Y. Pang, X. Y. Sun, D. Y. Yan, Y. F. Zhou, *Macromol. Rapid Commun.* **2012**, *33*, 767.
[45] H. Ghanbari, B. G. Cousins, A. M. Seifalian, *Macromol. Rapid Commun.* **2011**, *32*, 1032.
[46] C. C. Cheng, Y. C. Yen, F. C. Chang, *Macromol. Rapid Commun.* **2011**, *32*, 927.
[47] L. Cui, D. Y. Chen, L. Zhu, *ACS Nano* **2008**, *2*, 921.
[48] S. W. Kuo, R. S. Cheng, *Polymer* **2009**, *50*, 177.
[49] K. W. Huang, S. W. Kuo, *Macromol. Chem. Phys.* **2012**, *213*, 1509.
[50] W. H. Hu, K. W. Huang, C. W. Chiou, S. W. Kuo, *Macromolecules* **2012**, *45*, 9020.
[51] Y. C. Wu, S. W. Kuo, *Polym. Chem.* **2012**, *3*, 3100.
[52] W. B. Zhang, Y. Li, X. Li, X. Dong, X. Yu, C. L. Wang, C. Wesdemiotis, R. P. Quirk, S. Z. D. Cheng, *Macromolecules* **2011**, *44*, 2589.
[53] Y. C. Lin, S. W. Kuo, *Polym. Chem.* **2012**, *3*, 162.
[54] Y. C. Lin, S. W. Kuo, *Polym. Chem.* **2012**, *3*, 882.
[55] T. Kwei, *J. Polym. Sci., Polym. Lett. Ed.* **1984**, *22*, 307.
[56] E. Kim, H. Ahn, D. Y. Ryu, W. Joo, J. K. Kim, J. Jung, T. Chang, *Macromolecules* **2008**, *41*, 9875.
[57] Y. Kyogoku, R. C. Lord, A. Rich, *J. Am. Chem. Soc.* **1967**, *89*, 496.
[58] B. D. Mather, M. B. Baker, F. L. Beyer, M. A. G. Berg, M. D. Green, T. E. Long, *Macromolecules* **2007**, *40*, 6834.
[59] R. J. Roe, *Methods of X-ray and Neutron Scattering in Polymer Science*, Oxford University Press, New York **2000**.
[60] T. Hashimoto, H. Tanaka, H. Hasegawa, *Macromolecules* **1990**, *23*, 4378.
[61] T. Tanaka, H. Hasegawa, T. Hashimoto, *Macromolecules* **1991**, *24*, 240.